



1 Quantifying the uncertainty of precipitation forecasting 2 using probabilistic deep learning

3 Lei Xu¹, Nengcheng Chen^{1,2}, Chao Yang¹

4 ¹National Engineering Research Center for Geographic Information System, School of Geography and
5 Information Engineering, China University of Geosciences (Wuhan), Wuhan 430074, China

6 ²State Key Laboratory of Information Engineering in Surveying, Mapping, and Remote Sensing, Wuhan
7 University, Wuhan 430079, China

8 *Correspondence to:* Chao Yang (yangchao@cug.edu.cn)

9 Abstract. Precipitation forecasting is an important mission in weather science. In recent years, data-
10 driven precipitation forecasting techniques could complement numerical prediction, such as precipitation
11 nowcasting, monthly precipitation projection and extreme precipitation event identification. In data-
12 driven precipitation forecasting, the predictive uncertainty arises mainly from data and model
13 uncertainties. Current deep learning forecasting methods could model the parametric uncertainty by
14 random sampling from the parameters. However, the data uncertainty is usually ignored in the forecasting
15 process and the derivation of predictive uncertainty is incomplete. In this study, the input data uncertainty,
16 target data uncertainty and model uncertainty are jointly modeled in a deep learning precipitation
17 forecasting framework to estimate the predictive uncertainty. Specifically, the data uncertainty is
18 estimated a priori and the input uncertainty is propagated forward through model weights according to
19 the law of error propagation. The model uncertainty is considered by sampling from the parameters and
20 is coupled with input and target data uncertainties in the objective function during the training process.
21 Finally, the predictive uncertainty is produced by propagating the input uncertainty and sampling the
22 weights in the testing process. The experimental results indicate that the proposed joint uncertainty
23 modeling and precipitation forecasting framework exhibits comparable forecasting accuracy with
24 existing methods, while could reduce the predictive uncertainty to a large extent relative to two existing
25 joint uncertainty modeling approaches. The developed joint uncertainty modeling method is a general
26 uncertainty estimation approach for data-driven forecasting applications.

27 **1 Introduction**

28 Precipitation is a key hydrometeorological variable in earth system science, and is the main driving



29 factor of floods and droughts (Xu et al., 2019). In the year of 2019, the flood disaster driven by extreme
30 precipitation caused a direct economic loss of 29.6 billion dollars in China, and the drought disaster led
31 to a crop production loss of 23.6 billion kilograms (<http://www.mwr.gov.cn/sj/#tjgb>). Accurate
32 precipitation forecasting is vital for the early warning of flood and drought, smart city management and
33 agricultural water resources allocation (Van Den Hurk et al., 2012; Pozzi et al., 2013). However, the
34 precipitation forecasting problem suffers from uncertainties from data, algorithms and random factors
35 (Reeves et al., 2014; Kobold and Sušelj, 2005; Xu et al., 2020b). The predictive uncertainty is a
36 measurement of the spread of precipitation forecasting and could indicate how much the forecasted
37 precipitation values fluctuate around the mean (Papacharalampous et al., 2020). Therefore, the
38 uncertainty range should be given when generating precipitation forecasting results.

39 The precipitation forecasting methods can be divided into two categories: numerical weather
40 forecasting and statistical machine learning. Numerical models consider the physical process of earth
41 system and could simulate the interactions between atmospheres, oceans and lands (Sikder and Hossain,
42 2016; Molinari and Dudek, 1992). Numerical models have strong physical meaning and are the dominant
43 ways of operational precipitation forecasting. However, the forecasting ability of numerical models is
44 limited due to the uncertainty in initial and boundary conditions, the imperfection of parameterization
45 schemes and the uncertainty in parameters (Reeves et al., 2014). With the development of computer
46 technology and machine learning algorithms, using random data-driven techniques for precipitation
47 forecasting is becoming popular in recent years (Shi et al., 2015; Trebing et al., 2021; Sønderby et al.,
48 2020). The accuracy of data-driven methods is comparable to currently advanced numerical models in
49 short-term (e.g. from hours to weeks) precipitation forecasting. For example, the convolutional long-
50 short term memory network is shown to outperform the physical optical flow method in precipitation
51 nowcasting based on radar images (Shi et al., 2015). Another deep learning model called MetNet showed
52 advantages over traditional numerical models in terms of the forecasting accuracy and running time for
53 hourly precipitation prediction (Sønderby et al., 2020). The data-driven methods also exhibit appealing
54 results in subseasonal to seasonal precipitation forecasting relative to numerical models (Boukabara et
55 al., 2019; Chantry et al., 2021; Hwang et al., 2019). A key drawback of data-driven precipitation
56 forecasting method is the lack of physical meaning, also known as black-box model. Despite this feature,
57 data-driven statistical machine learning methods have been widely used for parameter calibration, data



58 processing, submodel replacement and process understanding among physical simulations (Ardabili et
59 al., 2019; Sahoo et al., 2017; Reichstein et al., 2019). The data-driven learning techniques are strong
60 complements to numerical models for the improvement of precipitation forecasting accuracy.

61 The predictive uncertainty in precipitation forecasting arises mainly from data and models (Gal,
62 2016). The data uncertainty comes from external observation conditions, instruments and processing
63 algorithms. The data uncertainty is usually examined by perturbing initial conditions in numerical models
64 and producing a perturbed multi-model ensemble, which is widely seen in hydrometeorological ensemble
65 forecasting (Xu et al., 2019; Gneiting and Raftery, 2005; Duan et al., 2019; Vitart et al., 2017). The data
66 uncertainty is rarely investigated in data-driven precipitation forecasting and is often assumed to be
67 accurate without error. The model uncertainty is often represented by an ensemble of perturbed model
68 physics and parameters in numerical weather forecasting (Vitart et al., 2017; Kirtman et al., 2014; Taylor
69 et al., 2012). In data-driven models, the model uncertainty is generally modeled by random regularization
70 of parameters (Gal, 2016; Kendall and Gal, 2017). For linear regression, the parametric uncertainty is
71 indicated by the standard deviation of trained parameters. In deep learning, the network layers could be
72 randomly abandoned to prevent overfitting and generate a forecasted ensemble by Monte Carlo sampling
73 (Kendall and Gal, 2017; Srivastava et al., 2014; Loquercio et al., 2020; Ghahramani, 2015).

74 The data and model uncertainties should be considered jointly in an integrated modeling framework
75 to get the predictive uncertainty, as the data and model uncertainties could both inflate the predictive
76 spread considerably (Gal, 2016; Kendall and Gal, 2017). It is expected that, the forecasting result would
77 be more or less different if the used data and parameters are randomly sampled from the population. Data
78 uncertainty is usually assumed as a constant or Gaussian distribution and could be propagated into final
79 forecasting through error forward propagation (Loquercio et al., 2020; Xu et al., 2020a). If the data
80 uncertainty is unknown, it can be learned from the training process by considering the data uncertainty
81 as a trainable parameter (Kendall and Gal, 2017). However, the joint learning of data errors and model
82 weights will increase the number of training parameters and may mix the error flow from data and
83 parameters. A prior estimation of data uncertainty could help unravel the data error and facilitate the
84 training process. On the other hand, previous forecasting studies usually model the input data uncertainty
85 and ignore the uncertainty in the target (predictand) data (Kendall and Gal, 2017; Loquercio et al., 2020).
86 The uncertainty in the target dataset also plays an important role in the parameter training process and



87 could influence the forecasting accuracy.

88 There are two ways to estimate the data uncertainty. One is to use in-situ ground stations to calculate
89 the systematic and random errors within the data and the other is to use multisource datasets to compute
90 random error by intercomparison (Xu et al., 2021; Gruber et al., 2016; Sun et al., 2018). The in-situ
91 validation method is limited to the number and density of ground stations and are suitable for small areas
92 with enough station coverage. The second method is independent of the in-situ stations and requires
93 multisource datasets with independent error distribution (Gruber et al., 2016). There are numerous
94 precipitation datasets from various sensors and models and could be used to calculate precipitation data
95 error at a large spatial scale (Xu et al., 2020b; Sun et al., 2018). Three-cornered hat (TCH) and triple
96 collocation (TC) are two commonly used methods to evaluate the random error among multisource
97 datasets, which do not require ground measurements as references (Premoli and Tavella, 1993; Mccoll
98 et al., 2014; Stoffelen, 1998). The basic assumption of TCH and TC methods is the stationarity of both
99 the raw dataset and its error, which may not be always satisfied for real-world data. Most of the existing
100 studies assume that the used multisource datasets obey the stationarity condition when using TCH or TC
101 methods (Xu et al., 2020b; Gruber et al., 2016; Gruber et al., 2017), which is useful for the determination
102 of relative prior random error.

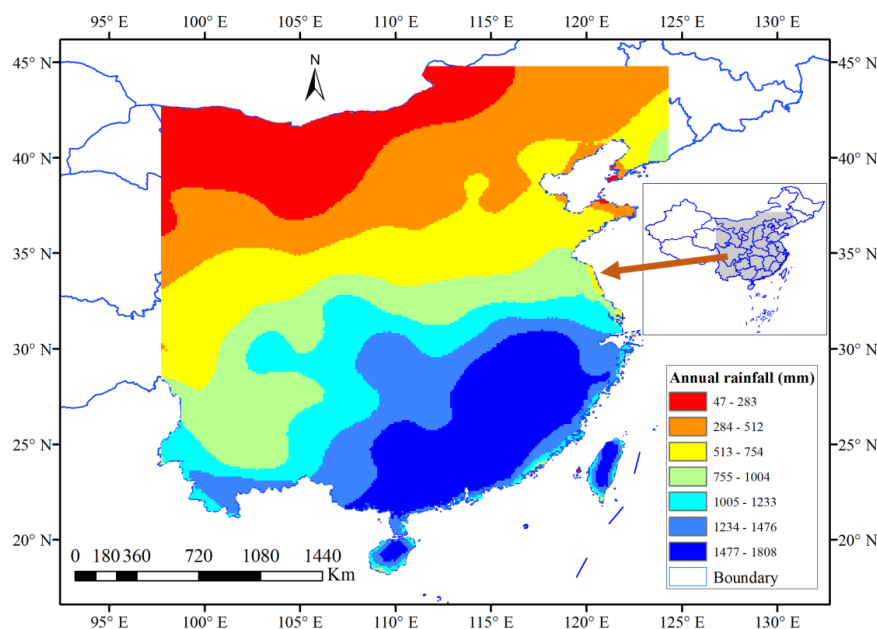
103 In this study, we aim to quantify the predictive uncertainty of data-driven precipitation forecasting
104 by fully considering the uncertainty from data and models. The data uncertainty is estimated by the TCH
105 method a priori and is assumed as Gaussian distribution. The data uncertainty is propagated within model
106 training by the law of error propagation. The parametric uncertainty is modeled by randomly abandoning
107 some network layers during the training process. The data and model uncertainties are jointly considered
108 in the objective function within a deep learning encoder-decoder framework. The forecasting
109 experiments are conducted to see whether the accuracy of precipitation forecasting can be improved by
110 joint data-model uncertainty modeling relative to several uncertainty processing strategies from the
111 existing studies.

112 **2 Study area and data**

113 The study area is located at southern and northern China, East Asia (Figure 1). The annual rainfall
114 decreases from the southeast to the northwest, with an approximately average rainfall of 1500 mm in the



115 southeast regions and 300 mm in the northwest areas. Most of the southern areas feature a subtropical
116 monsoon climate and the rainfall is relatively larger in summer and smaller in winter. From June to July
117 in 2020, extreme precipitation hit the southern China (Wei et al., 2020) and caused a direct economic
118 loss of 13.2 billion dollars. The precipitation forecasting in southern area of China is very challenging
119 and meaningful. Previous studies use numerical models for precipitation forecasting in this area and show
120 some values (Yuan et al., 2012; Luo et al., 2017). The northern area of China features the temperate moon
121 and continental climates, with an annual rainfall of 400 to 800 mm and the main rainy season of July and
122 August. Here we would like to explore the possibility of weekly precipitation forecasting by a data-driven
123 deep learning method.



124
125 Figure 1: The study area for short-term precipitation forecasting.

126 Multisource precipitation datasets are used here to obtain the data error and to measure the
127 precipitation forecasting ability of different uncertainty processing strategies, including the Modern-Era
128 Retrospective Analysis for Research and Applications, version 2 (MERRA-2) (Gelaro et al., 2017), the
129 National Centers for Environmental Prediction Reanalysis version 2 (NCEP R2) (Saha et al., 2014) and
130 the European Centre for Medium-Range Weather Forecasts Reanalysis version 5 (ERA-5) (Hersbach et
131 al., 2020) datasets from 1980 to 2020. The surface 2-meter temperature and the geopotential height at
132 500 hPa datasets are collected from the three datasets accordingly as predictors. All these daily datasets



133 are converted to weekly data and are bilinearly interpolated into 0.25° resolution. In the forecasting
134 process, the temperature and geopotential height predictors in the historical three consecutive weeks are
135 used to forecast the precipitation in the target week.

136 **3 Methods**

137 **3.1. Estimation of data uncertainty**

138 The TCH method (Xu et al., 2020b; Premoli and Tavella, 1993) is used to estimate the uncertainty
139 in temperature, geopotential height and precipitation datasets. The collected three datasets are all
140 reanalysis data, which is generated from different physical models and data assimilation algorithms. The
141 different reanalysis datasets and their errors are generally not closely correlated and are regarded as
142 collocated datasets for the uncertainty estimation, similar with existing studies (Xu et al., 2021; Mccoll
143 et al., 2014; Gruber et al., 2017). In the TCH algorithm, one arbitrary dataset is chosen as the reference
144 among the three datasets, and then the differencing operation is conducted between the reference and the
145 other two datasets to get the differencing series. The covariance of the differencing series is connected
146 to the variance-covariance matrix of precipitation datasets through matrix transformation. The
147 parameters of the variance-covariance matrix are iteratively resolved by minimizing the global
148 correlation of the covariance of the differencing series. A detailed introduction of TCH method could
149 refer to Premoli and Tavella (1993) and Xu et al. (2020b).

150 The uncertainties of the predictors and predictands are estimated seasonally by the TCH method.
151 The weekly datasets are grouped according to the weekly climatology and then used to estimate the
152 uncertainty. For example, all the precipitation datasets which belongs to the first week of each year are
153 concatenated to apply the TCH method in order to get the uncertainty of the datasets on the first week of
154 each year. Similarly, the data uncertainty on the second week, third week and until the fifty-two week is
155 evaluated sequentially. This strategy enables a time-variant uncertainty estimation, which is more
156 reasonable as the precipitation climatology is different for different seasons. The NECP R2 and ERA-5
157 data are used to assist the uncertainty estimation of MERRA-2 data by the TCH method, and the
158 precipitation forecasting experiments are conducted based on MERRA-2 data to evaluate the proposed
159 forecasting framework.



160 **3.2. Variational Bayesian inference**

161 Here we introduce the variational inference theory (Hoffman et al., 2013), which is a standard
162 Bayesian modeling technique for the estimation of model uncertainty. Given the input data $X=\{x_1, \dots, x_N\}$
163 and the output data $Y=\{y_1, \dots, y_N\}$, the Bayesian regression is to find suitable parameters within the
164 function $y=f^w(x)$ which could generate the output Y according to the input X . The parameters w is assumed
165 to obey a prior distribution $p(w)$ before the observations are known. When the observed data is obtained,
166 it is possible to determine which parameters are more suitable for the function according to the data. A
167 likelihood distribution $p(y|x, w)$ is defined to describe the probability of y generated by x and w . For
168 example, a Gaussian likelihood function is defined as

$$169 \quad p(y|x, w) = \mathcal{N}(y; f^w(x), \tau^{-1}I)$$

170

171

172

173

(1)

174 where τ^{-1} is the observation noise.

175 Given the input data X and the output data Y , the Bayesian theorem is to find the posterior
176 distribution of parameters in the parameter space.

$$177 \quad p(w|X, Y) = \frac{p(Y|x, w)p(w)}{p(Y|X)}$$

178

179

180

181

(2)

182 where the numerator $p(Y|X)$ is the normalization factor, also named as model evidence.

$$183 \quad p(Y|X) = \int p(Y|X, w)p(w)dw$$

184

185



186
187 (3)

188 The solution of Equation (3) needs to marginalize the likelihood over w , which is tractable
189 analytically for some simple models such as Bayesian regression, while is intractable for complex models
190 such as deep learning methods (Gal, 2016).

191 Given the new input data x' , the forecasted value is generated by the integral of probability over the
192 parameter space, which is called the inference process.

193
$$p(y'|x', X, Y) = \int p(y'|x', w)p(w|X, Y)dw$$

194
195
196
197 (4)

198 Since the posterior distribution of parameters $p(w|X, Y)$ cannot be obtained analytically, an
199 approximate analytical distribution $q_{\theta}(w)$ could be defined, with θ as the parameter to be estimated, to
200 be as close as the posterior distribution. The Kullback-Leibler (K-L) divergence (Kullback and Leibler,
201 1951) is an indicator to measure the similarity of two distributions, also known as relative entropy. The
202 objective function is to minimize the K-L divergence between the two distributions.

203
$$KL(q_{\theta}(w)||p(w|X, Y)) = \int q_{\theta}(w) \log \frac{q_{\theta}(w)}{p(w|X, Y)} dw$$

204
205
206
207 (5)

208 The optimal variational distribution $q'_{\theta}(w)$ is obtained when the K-L divergence is minimized.
209 The estimated variational distribution could be regarded as the posterior distribution of parameters and
210 then the predictive distribution could be generated.



$$p(y'|x', X, Y) \approx \int p(y'|x', w)q'_\theta(w)dw =: q'_\theta(y'|x')$$

211
212
213 (6)

214 The above inference process is the variational Bayesian inference. Variational inference replaces
215 the integral of the likelihood with optimization, which simplifies the estimation of posterior distribution.

216 3.3. Monte Carlo sampling

217 Monte Carlo method is a kind of stochastic simulation technology, proposed by Stanislaw Ulam
218 and John von Neumann during the second world war (Von Neumann and Ulam, 1951). Monte Carlo
219 methods are used to estimate unknown parameters by random sampling and are widely applied in
220 mathematics, physics, game theory and finance (Brooks, 1998; Jacoboni and Lugli, 2012; Metropolis
221 and Ulam, 1949; Rubinstein and Kroese, 2016).

222 In Equation (4), the posterior distribution $p(w|X, Y)$ cannot be solved analytically. Assume U_i as the
223 weight matrix $K_i \times K_{i-1}$ from $i-1$ layer to i layer, i.e. $w = \{U_i\}_{i=1, \dots, L}$, a variational weight distribution $q(w)$
224 is defined to randomly replace the columns with zero (dropout process).

$$U_i = H_i \cdot \text{diag}\left([z_{i,j}]_{j=1}^{K_i}\right)$$

225
226
227 (7)

$$[z_{i,j}] \sim \text{Bernoulli}(p_i), i = 1, \dots, L, j = 1, \dots, K_{i-1}$$

228
229
230 (8)

231 where p_i and H_i are variational parameters; $z_{i,j}$ is a binary variable, with a value of zero representing the
232 abandoning of j th unit in $i-1$ layer and a value of one the keeping, based on the *Bernoulli* distribution at
233 the probability p_i .

234 The predictive distribution is estimated after minimizing the K-L divergence.

$$235 q(y'|x') = \int p(y'|x', w)q(w)dw$$



236
 237 (9)

238 The predictive mean and variance can be obtained after repeating the dropout process multiple times.

239 $\mathbb{E}_{q(y'|x')}(y') = \int y' q(y'|x') dy' =$
 240 $\int y' \mathcal{N}(y'; \hat{y}'(x', U_1, \dots, U_L), \tau^{-1}I) \text{Bern}(U_1) \cdots \text{Bern}(U_L) dU_1 \cdots dU_L dy' =$
 241 $\int \hat{y}'(x', U_1, \dots, U_L) \text{Bern}(U_1) \cdots \text{Bern}(U_L) dU_1 \cdots dU_L \approx \frac{1}{T} \sum_{t=1}^T \hat{y}'(x', \hat{U}_{1,t}, \dots, \hat{U}_{L,t})$
 242
 243 (10)

244 $\text{Var}_{q(y'|x')}(y') \approx \tau^{-1}I + \frac{1}{T} \sum_{t=1}^T \hat{y}'(x', \hat{U}_{1,t}, \dots, \hat{U}_{L,t})^T \hat{y}'(x', \hat{U}_{1,t}, \dots, \hat{U}_{L,t}) -$
 245 $\mathbb{E}_{q(y'|x')}(y')^T \mathbb{E}_{q(y'|x')}(y')$
 246 (11)

247 where $u_{t,i}$ is the forecasted value for i th pixel and t th ensemble. The calculation of predictive variance
 248 is based on the standard deviation of the ensemble, which represents the spread of the forecasted values.

249 The above Monte Carlo sampling and dropout process is the Monte Carlo dropout technique, which
 250 is used to obtain the model uncertainty here.

251 3.4. Joint data and model uncertainties modeling

252 Dropout is a Bayesian method to model the model uncertainty in forecasting (Srivastava et al.,
 253 2014). However, the data uncertainty also needs to be considered. Kendall and Gal (2017) regarded the
 254 data uncertainty as a trainable parameter and jointly considered data and model uncertainties. However,
 255 the predictand data uncertainty is ignored and the learning of data uncertainty increases the number of
 256 training parameters. Here we propose an integrated modeling framework to fully incorporate the data
 257 and model uncertainties during the training process (Figure 2). First, the data uncertainties of predictors
 258 and predictands are estimated by the TCH method and are assumed as Gaussian distribution.

259 $\sigma = TCH(D_i), i = 1, 2, 3$

260



261 (12)

262 $\sigma_x \sim \mathcal{N}(0, \sigma)$

263

264 (13)

265 $\sigma_y \sim \mathcal{N}(0, \sigma)$

266

267 (14)

268 The data uncertainty is randomly sampled T times to generate an ensemble of predictors and
 269 predictands. In the meantime, the parameters are randomly dropped out for T times to construct a
 270 parametric ensemble. The perturbed data and parameter values are jointly used to calculate the training
 271 loss. The objective function is expressed as follows (Kendall and Gal, 2017), which is obtained from the
 272 likelihood of a Gaussian process (Srivastava et al., 2014).

273
$$\mathcal{L}(\theta, p) = -\frac{1}{N} \sum_{i=1}^N \log p(y_{i,\sigma} | f^{\theta_i}(x_{i,\sigma})) + \frac{1-p}{2N} \|\theta\|^2$$

274

275 (15)

276
$$\sigma = \sqrt{(\sigma_x^{(l)})^2 + \sigma_y^2}$$

277

278 (16)

279 where N is the sample size; p is the dropout probability; $\theta_i \sim q'_\theta(U)$; θ is the parameter to be estimated;
 280 σ_x and σ_y are the data uncertainty for predictor and predictand, respectively. The negative log-likelihood
 281 function can be deduced according to the objective function.

282
$$-\log p(y_{i,\sigma} | f^{\theta_i}(x_{i,\sigma})) \propto \frac{1}{2\sigma^2} \|y_i - f^{\theta_i}(x_i)\|^2 + \frac{1}{2} \log(\sigma^2)$$

283

284 (17)



285 where σ is the regression noise, with the mean of zero in a Gaussian distribution.

286 The objective function consists of a mean square error (MSE) term adjusted by data uncertainty and
287 a regularization term, which is the negative logarithm of the Gaussian likelihood function. The objective
288 function includes an uncertainty parameter σ^2 , which is determined by the sum of propagated uncertainty
289 and target data uncertainty. The minimization of the negative log-likelihood function could be reached
290 by differentiating the optimization function and setting to zero.

$$291 \quad \frac{\partial}{\partial \sigma^2} \left[\frac{1}{2\sigma^2} \|y_i - f^{\theta_i}(x_i)\|^2 + \frac{1}{2} \log(\sigma^2) \right] = 0$$

292

293 (18)

$$294 \quad \Rightarrow -\frac{1}{2\sigma^4} \|y_i - f^{\theta_i}(x_i)\|^2 + \frac{1}{2\sigma^2} = 0$$

295

296 (19)

$$297 \quad \Rightarrow \sigma^2 = \|y_i - f^{\hat{\theta}_i}(x_i)\|^2$$

298

299 (20)

300 where the minimum value of the negative log-likelihood function could be reached when the data
301 variance equals to the square of the difference between the forecasted value and the observation.

302 Once the network weights are determined according to the objective function, the new input data
303 uncertainty is propagated and the weights are randomly sampled to produce the forecasted ensemble.
304 The predictive mean and variance are calculated from the predictive ensembles.

$$305 \quad \mu_i = \frac{1}{T} \sum_{t=1}^T y_{t,i}$$

306

307 (21)

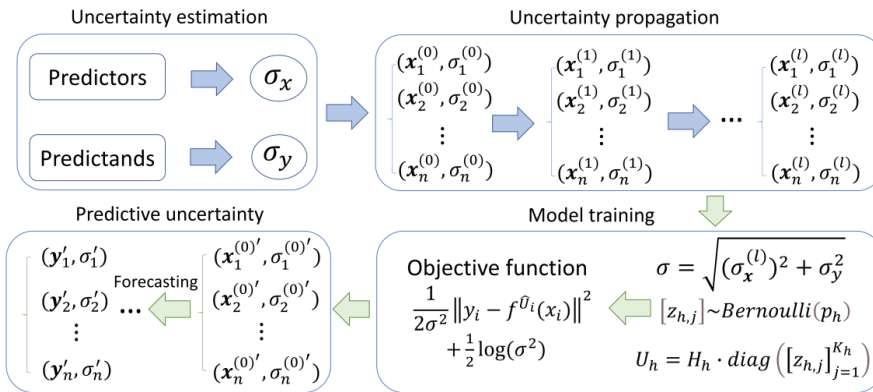
$$308 \quad \text{Var}_i \approx \frac{1}{T} \sum_{t=1}^T y_{t,i}^2 - \left(\frac{1}{T} \sum_{t=1}^T y_{t,i} \right)^2 + \frac{1}{T} \sum_{t=1}^T \sigma_{t,i}^2$$



309

310

(22)



311

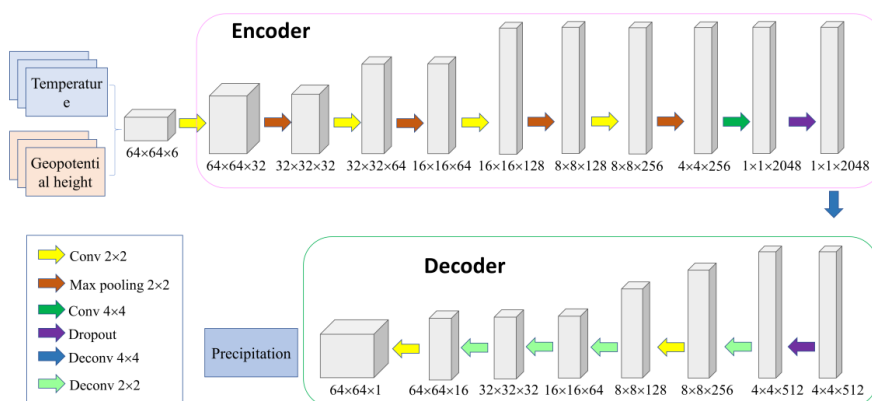
312 Figure 2: The proposed integrated data-model uncertainty modeling framework in precipitation
 313 forecasting.

314 **3.5. The deep learning forecasting framework**

315 In deep learning, encoder-decoder is a commonly used forecasting model (Badrinarayanan et al.,
 316 2017; Cho et al., 2014). In the encoder process, an input signal is converted into a one-dimension vector
 317 with fixed length. In the decoder process, the one-dimension vector is transformed into the target data
 318 with variable length. The available networks used for encoder and decoder processes are arbitrary and
 319 depend on the specific problem, such as convolutional neural network (CNN), recurrent neural network
 320 (RNN) and long-short term memory (LSTM) network (Hochreiter and Schmidhuber, 1997; Goodfellow
 321 et al., 2016). Here we designed a deep learning encoder-decoder model for weekly precipitation
 322 forecasting (Figure 3). The temperature and geopotential height data for previous three weeks are
 323 regarded as inputs, with an image size of $64 \times 64 \times 6$. In the encoder process, the input image is down-
 324 sampled by a series of convolution, pooling and dropout operations, resulting in a one-dimension vector
 325 ($1 \times 1 \times 2048$). In the decoder process, the one-dimension vector is up-sampled by deconvolution, dropout
 326 and convolution operations, resulting in a forecasted precipitation image ($64 \times 64 \times 1$). The down-sampling
 327 and up-sampling procedures are used to learn the nonlinear mapping relationships between predictors
 328 and predictands.



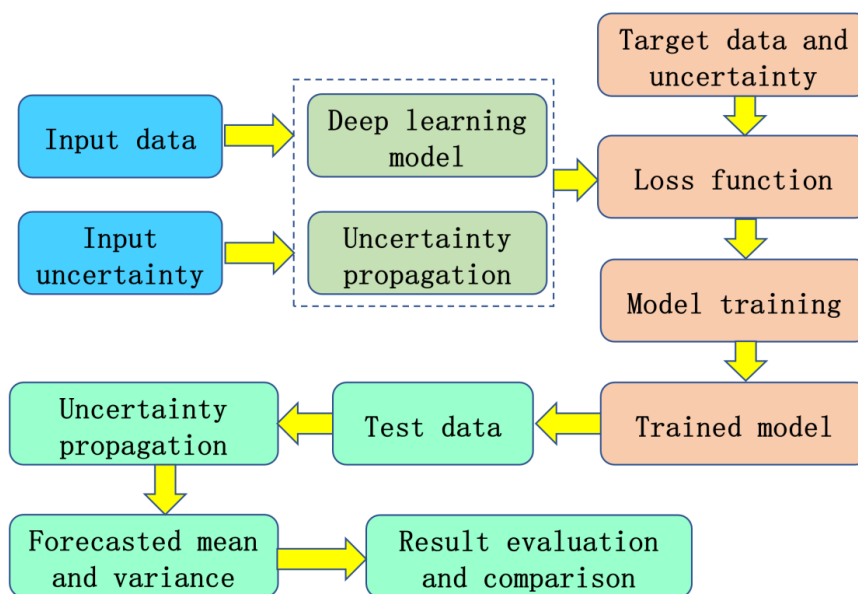
329 In the training process, the optimization algorithm is set to Adam (Kingma and Ba, 2014), which is
 330 a stochastic learning algorithm based on adaptive moment. The network learning rate is set to 0.001 and
 331 the stopping rule of iteration is that the validating error does not decrease for at least 100 times. The data
 332 uncertainty is propagated forward according to the law of uncertainty propagation and the dropout
 333 process is repeated 10 times with a dropout rate of 0.5. The random seed is set to 1 to enable the
 334 reproducibility of the experiment. The experimental data spans from 1980 to 2020 (2139 weeks), of
 335 which 60%, 20% and 20% of the data are used for training, validating and testing, respectively. The
 336 optimal model parameters are determined based on the minimal validating loss.



337

338 Figure 3: The developed deep learning model for precipitation forecasting.

339 The proposed deep learning framework for precipitation forecasting is demonstrated in Figure 4.
 340 The input data and its uncertainty are prepared and are considered as inputs for the forecasting model.
 341 The model weights are initialized and the input uncertainty is propagated forward according to the
 342 weights. The loss function value is calculated according to the forecasted value, the propagated
 343 uncertainty, target data and its uncertainty. The forecasting model is trained according to the optimization
 344 algorithm and then the trained model is obtained. Next the test data is used to produce the forecasted
 345 value and variance based on the model weights and uncertainty propagation. Finally, the forecasted value
 346 and variance are evaluated and compared with several precipitation forecasting methods.



347

348

Figure 4: The proposed deep learning framework for precipitation forecasting.

349

350

351

352

353

354

355

356

357

358

359

360

361

362

363

364

We designed a series of comparison experiments to investigate the effect of different uncertainty processing strategies on the forecasting performance. The precipitation forecasting experiment without considering uncertainty is used as the baseline (Experiment 1). The mean square error is used as the loss function and the data and model uncertainties are not considered in Experiment 1. The uncertainty sources are incorporated differently into the experiments, including predictor uncertainty (Experiment 2), predictor and predictand uncertainties (Experiment 3), model uncertainty based on Srivastava et al. (2014)'s method (Experiment 4), data and model uncertainties based on Kendall and Gal (2017)'s method (Experiment 5), data and model uncertainties based on Loquercio et al. (2020)'s method (Experiment 6), and data and model uncertainties (Experiment 7) based on the proposed framework here. The data uncertainty only includes the propagated uncertainty from the input data in Equation (16) in Experiment 2, while the propagated uncertainty from the input data and the target data uncertainty are both included in Experiment 3. In Experiment 4, the data uncertainty is ignored and the model parameters are randomly sampled for 10 times to get the model spread. In Experiment 5, the input uncertainty is regarded as the trainable parameter and the trained uncertainty value is used as the data uncertainty in Equation (16), and the model uncertainty is considered the same way as Experiment 4. In Experiment 6, the input data uncertainty is propagated and the model uncertainty is modeled by sampling the parameters. In



365 Experiment 7, the input uncertainty is propagated and the target data uncertainty is included in Equation
366 (16) and the model uncertainty is represented by multiple sampling process.

367 The root mean square error (RMSE) statistic is used to measure the difference between forecasted
368 value and true value.

$$369 \text{ RMSE} = \sqrt{\frac{\sum_{i=1}^n (y_i - \hat{y}_i)^2}{n}} \quad (23)$$

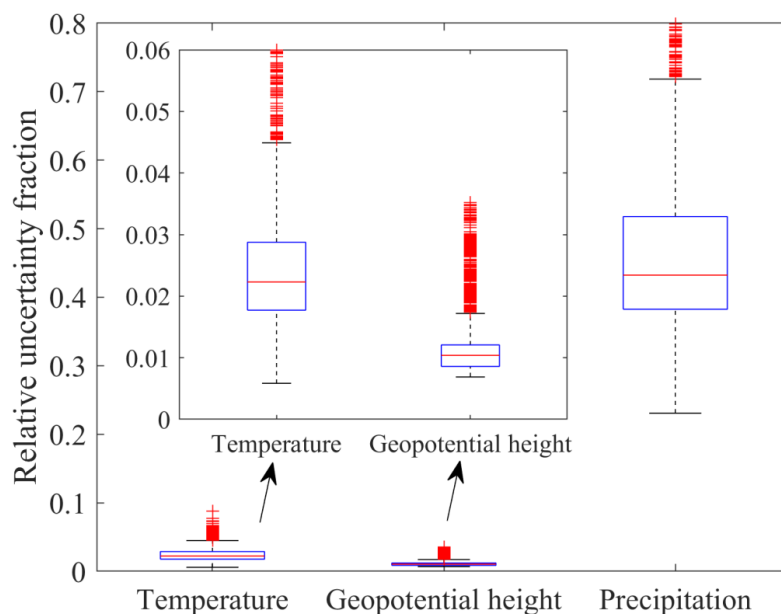
370
371

372 where y_i is the true value or observation and \hat{y}_i is the forecasted value; n is the sample size.

373 4 Results and discussion

374 4.1. The uncertainty of input and output datasets

375 The data uncertainty of predictors and predictand is calculated based on the TCH method and is
376 shown in Figure 5. The precipitation data uncertainty is much higher than



377



378 Figure 5: The data uncertainty calculated by the TCH method. The uncertainty distribution is plotted
379 according to the uncertainty over all the pixels of the study area. The red cross indicates the outliers.

380 the temperature and geopotential height variables, with a median of ~43% relative uncertainty fraction
381 for precipitation, ~2% for temperature and ~1% for geopotential height. Therefore, the precipitation data
382 suffer from greater uncertainty relative to the input data and the predictand uncertainty should not be
383 ignored in the training process. The combination of the propagated input uncertainty and the predictand
384 uncertainty is used as the adjusted parameter to regularize the loss function, which is relatively reasonable
385 as the data with larger uncertainty should contribute less to the total training loss. It should be noted that
386 the predictor and predictand data are normalized to [0,1] before uncertainty estimation to ensure a fair
387 comparison of uncertainty value. The high uncertainty for precipitation data is related to strong
388 spatiotemporal heterogeneity of precipitation and the high inconsistency among the reanalysis data (Xu
389 et al., 2020b), while temperature and geopotential height data are much more homogeneous in space and
390 time.

391 **4.2. Overall precipitation forecasting performance**

392 As for the predictive uncertainty, the forecasting method that only considers model uncertainty
393 (Srivastava et al., 2014) obtains the minimum predictive uncertainty (Table 1). However, the data
394 uncertainty is not considered when only sampling from the parameters and thus the impact of data error
395 on forecasting is not evaluated. In Kendall and Gal (2017)'s method, the data uncertainty is regarded as
396 a trainable parameter and the model uncertainty is modeled by random parameter sampling. Whether the
397 learned parameter value for data uncertainty parameter could represent the real data error needs further
398 investigation. Loquercio et al. (2020) used the law of uncertainty propagation to propagate the data
399 uncertainty and sampled the parameters randomly during training. In our proposed method, the input
400 data uncertainty, target data uncertainty and model uncertainty are jointly coupled by uncertainty
401 propagation and random parameter sampling. The average predictive uncertainty (3.460) based on the
402 proposed method is smaller than the Loquercio et al. (2020)'s and Srivastava et al. (2014)'s methods. In
403 this regard, the proposed method could reduce the predictive uncertainty of precipitation forecasting to
404 some extent, when jointly modeling data and model uncertainties. The proposed method could slightly
405 improve the precipitation forecasting performance and could improve the reliability of precipitation
406 forecasting by reducing the uncertainty.

407 When only the input uncertainty is modeled in the forecasting model, the predictive uncertainty is
408 12.950. If the target data uncertainty is coupled with input uncertainty, the predictive uncertainty is
409 substantially reduced (3.022). In Equation (20), when the predictive error on the right side of the equation
410 reaches local minimum and remains unchanged basically, the left side of the equation includes the input



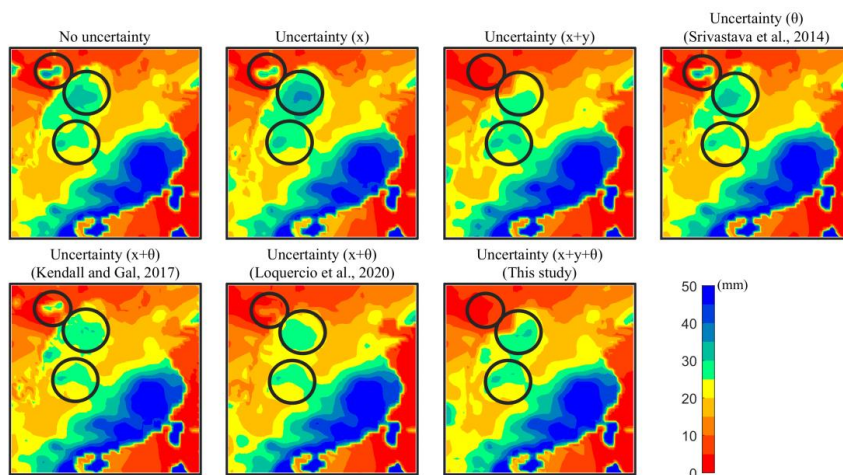
411 uncertainty propagation and the target data uncertainty. When new data is used to make prediction, the
412 predictive uncertainty is generated by the input uncertainty and the law of error propagation. Thus, when
413 only the input uncertainty is modeled in Equation (20), the left side of this Equation equals to the
414 propagated uncertainty from the input data. If the left side of the Equation (20) is replaced from the
415 propagated input uncertainty with the combination of propagated input uncertainty and target uncertainty,
416 the propagated input uncertainty after replacement will be smaller than that of no replacement, i.e.
417 $(\sigma_x^{(l)})^2 = \sigma^2 - \sigma_y^2 < \sigma^2 = \|y_i - f^{\theta_i}(x_i)\|^2$.

418 Table 1. The accuracy of precipitation forecasting based on different uncertainty processing strategies.
419 The best RMSE is shown in bold for each column.

Uncertainty processing	RMSE	Uncertainty
No uncertainty	25.357	-
Predictor uncertainty	25.500	12.950
Predictor and predictand uncertainties	25.932	3.022
Model uncertainty (Srivastava et al., 2014)	25.368	1.778
Data and model uncertainties (Kendall and Gal, 2017)	25.225	4.914
Data and model uncertainties (Loquercio et al., 2020)	25.324	13.169
Data and model uncertainties (This study)	25.199	3.460

420 4.3. Spatial patterns of precipitation forecasting

421 In Figure 6, the spatial patterns of the RMSE for precipitation forecasting demonstrate some
422 similarities and differences between different uncertainty processing strategies. Overall, the spatial
423 distribution of RMSE is similar with each other and is smaller in the northwest region but larger in the
424 southeast region. In the places where the annual rainfall is abundant, the water cycle process is
425 accelerated and the precipitation observations may suffer from large uncertainty. The difficulty of
426 forecasting extreme high precipitation volume also increases the average RMSE in the southeast region
427 relative to the northwest region (Yuan et al., 2012; Huang et al., 2013). There are some differences of the
428 forecasting error among different forecasting methods in local areas. For example, the forecasting
429 performance based on our proposed method could outperform the methods in Experiments 1, 2 and 4
430 and is comparable with the methods in Experiments 3, 5 and 6 for the local areas covered by black circles
431 in Figure 6.

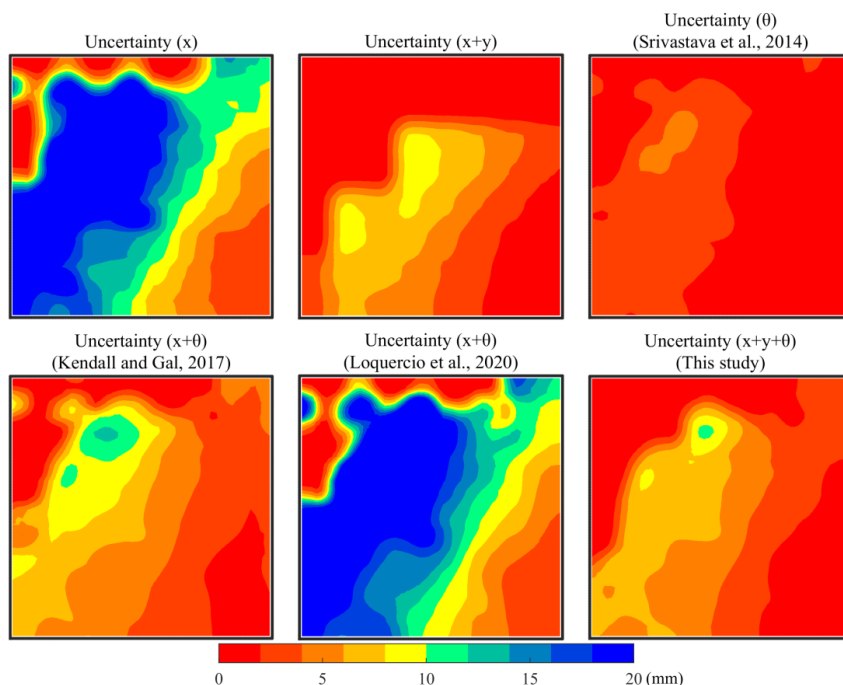


432

433 Figure 6: The spatial patterns of RMSE for precipitation forecasting. In this figure, x means the modeling
434 of input uncertainty; x+y represents the modeling of input and output uncertainty; x+y+θ indicates the
435 modeling of input uncertainty, output uncertainty and model uncertainty. The black circles represent the
436 highlighted areas.

437

438 Figure 7 demonstrates the impact of different uncertainty processing methods on the predictive
439 uncertainty of precipitation. If only the input uncertainty is considered in the forecasting model, the
440 predictive uncertainty is large in the central and southwest regions. The predictive uncertainty could be
441 substantially reduced when incorporating the target data uncertainty besides the input uncertainty. The
442 modeling of model uncertainty only could produce the minimum predictive uncertainty spatially in the
443 experiment. The predictive uncertainty is relatively small based on Kendall and Gal (2017)'s method. In
444 Loquercio et al. (2020)'s method, the predictive uncertainty is close to the result of input uncertainty
445 modeling in space, suggesting that the coupled modeling of input and model uncertainties fails to help
446 reduce the forecasting spread. Our proposed method could include the input, target and model
447 uncertainties jointly and could help reduce the predictive uncertainty to a large extent, relative to the
448 methods in Experiment 2 and 6.



449

450

Figure 7: The spatial patterns of uncertainty for precipitation forecasting.

451 4.4. Uncertainty analysis and discussion

452 In precipitation forecasting, data and model uncertainties both bring uncertainty to the forecasting
453 result. The higher the data and model uncertainties, the more divergent the forecasting, suggesting the
454 forecasting less reliable. Therefore, the data and model uncertainties should be jointly considered in the
455 forecasting process (Gal, 2016; Kendall and Gal, 2017; Loquercio et al., 2020; Parrish et al., 2012).
456 Although the predictive error is close to each other among different forecasting methods in Figure 6 and
457 Table 1, the predictive uncertainty has some discrepancies. The modeling of input uncertainty only in the
458 forecasting model would bring high predictive uncertainty and ignore the target data uncertainty. The
459 joint modeling of input and target uncertainties could reduce the predictive uncertainty substantially,
460 which is related to the change of the variance in Equations (16) and (20) corresponding to the minimum
461 value of the forecasting error term. The propagation of input uncertainty is constrained by refining the
462 uncertainty representation in Equation (16) after incorporating the target uncertainty term and thus
463 changing the weight training process.

464 The proposed method in this study could model the input uncertainty, target uncertainty and model



465 uncertainty jointly and could reduce the predictive uncertainty relative to Kendall and Gal (2017)'s and
466 Loquercio et al. (2020)'s methods. The developed method does not increase the training parameter and
467 is a general forecasting uncertainty method for geophysical applications such as temperature forecasting,
468 runoff forecasting and wind speed forecasting, especially for data-driven forecasting models (Ham et al.,
469 2019; Zheng et al., 2020; Hossain et al., 2015).

470 In numerical precipitation forecasting systems, ensemble forecasting is commonly used to quantify
471 the predictive uncertainty (Duan et al., 2019). In ensemble forecasting, the model parameters and data
472 are perturbed to produce a forecasted ensemble and thus the data and model uncertainties are both
473 considered. However, it would be time-consuming and cost-expensive to conduct large-sample sampling
474 for complex physical models. In our developed method, the law of error propagation is used to propagate
475 the data uncertainty. The uncertainty propagation of convolution, max-pooling and deconvolution in the
476 deep learning forecasting model is tractable in an analytical form. However, the uncertainty propagation
477 process is generally intractable analytically for complex statistical or physical models. Therefore, the
478 theory and implementation technology for uncertainty modeling require further development, such as
479 surrogate modeling, Monte Carlo methods, polynomial chaos expansions and Bayesian approaches
480 (Linde et al., 2017; Sudret et al., 2017; Zhu and Zabaras, 2018; Schiavazzi et al., 2017; Nitzler et al.,
481 2020).

482 **5 Conclusion**

483 In this study, we proposed a data-model uncertainty coupling framework to estimate the predictive
484 uncertainty of precipitation forecasting. In this framework, the predictor and predictand uncertainties are
485 estimated a priori by the TCH method and are assumed as Gaussian distribution. The predictor uncertainty
486 is propagated forward during training and testing processes by the law of error propagation. The model
487 uncertainty is represented by randomly abandoning model weights from deep learning layers. The data
488 and model uncertainties are jointly modeled in the objective function during training and are also used
489 during the testing process. The loss function is constructed by the MSE statistic adjusted by data
490 uncertainty and a regularization term based on logarithmic data uncertainty. In the loss function, the
491 adjusting parameter is determined by the combination of the square of predictor and predictand
492 uncertainties. The forecasted ensembles are used to calculate the predictive mean and variance to estimate



493 the predictive uncertainty of precipitation.

494 The weekly precipitation forecasting in southern and northern China is used as an example to
495 examine the effectiveness of the proposed joint uncertainty modeling framework. Temperature and
496 geopotential height data in previous three weeks are used to forecast the precipitation in the target week.
497 The forecasting model is developed based on an encoder-decoder deep neural network, with multivariate
498 spatiotemporal predictor data as inputs and spatiotemporal precipitation data as output. The results
499 exhibit comparable precipitation forecasting accuracy for the proposed method with several existing
500 uncertainty processing strategies, while the predictive uncertainty is reduced relative to two data-model
501 uncertainty modeling methods. The reduction of predictive uncertainty is significant for quantitative
502 precipitation forecasting from a data-driven view.

503 The data-driven precipitation forecasting method has limitations in the interpretation part relative
504 to numerical weather prediction. The precipitation forecasting accuracy for numerical models could still
505 be improved by improving the parameterization schemes and resolving the uncertainties in observations,
506 parameters and models. The proposed uncertainty modeling framework may also provide some insights
507 for the uncertainty quantification in numerical prediction models. For example, the uncertainty
508 propagation for the input data and the coupling with target data uncertainty could be used in a data
509 assimilation scheme to estimate the propagated uncertainty in weather forecasting.

510 Data-driven precipitation forecasting could be used as a tool to assist regional prediction and
511 warning of extreme weather events together with numerical models. The proposed joint data-model
512 uncertainty modeling framework could help estimate the forecasting spread and is a general approach to
513 derive predictive uncertainty for geophysical forecasting applications. Further research should focus on
514 the non-Gaussian uncertainty modeling for complex integrated statistical-physical models.

515 **Data availability**

516 The meteorological data are publicly available and can be obtained via the website <https://gmao.gsfc.nasa.gov/reanalysis/MERRA-2/> for MERRA-2, https://psl.noaa.gov/data/gridded/data.ncep_reanalysis2.html for NCEP R2 and <https://climate.copernicus.eu/climate-reanalysis> for ERA-5.



519 **Author contributions**

520 LX conceptualized and wrote the paper. CY provided supervision of this study. NC gave support
521 in developing the manuscript.

522 **Competing interests**

523 The authors declare that they have no conflict of interest.

524 **Acknowledgment**

525 This research was supported by the National Key R&D Program (2018YFB2100500) and the National
526 Natural Science Foundation of China program (41890822).

527 **References**

- 528 Ardabili, S., Mosavi, A., Dehghani, M., and Várkonyi-Kóczy, A. R.: Deep learning and machine
529 learning in hydrological processes climate change and earth systems a systematic review,
530 International Conference on Global Research and Education, 52-62,
531 Badrinarayanan, V., Kendall, A., and Cipolla, R.: SegNet: A Deep Convolutional Encoder-Decoder
532 Architecture for Image Segmentation, IEEE Transactions on Pattern Analysis and Machine
533 Intelligence, 39, 2481-2495, 10.1109/TPAMI.2016.2644615, 2017.
534 Boukabara, S.-A., Krasnopolsky, V., Stewart, J. Q., Maddy, E. S., Shahroudi, N., and Hoffman, R. N.:
535 Leveraging modern artificial intelligence for remote sensing and NWP: Benefits and challenges, B.
536 Am. Meteorol. Soc., 100, ES473-ES491, 2019.
537 Brooks, S.: Markov chain Monte Carlo method and its application, Journal of the royal statistical
538 society: series D (the Statistician), 47, 69-100, 1998.
539 Chantry, M., Christensen, H., Dueben, P., and Palmer, T.: Opportunities and challenges for machine
540 learning in weather and climate modelling: hard, medium and soft AI, 2021.
541 Cho, K., Van Merriënboer, B., Bahdanau, D., and Bengio, Y.: On the properties of neural machine
542 translation: Encoder-decoder approaches, arXiv preprint arXiv:1409.1259, 2014.
543 Duan, Q., Pappenberger, F., Wood, A., Cloke, H. L., and Schaake, J.: Handbook of
544 hydrometeorological ensemble forecasting, Springer2019.
545 Gal, Y.: Uncertainty in deep learning, University of Cambridge, 1, 4, 2016.
546 Gelaro, R., McCarty, W., Suárez, M. J., Todling, R., Molod, A., Takacs, L., Randles, C. A., Darmenov,
547 A., Bosilovich, M. G., and Reichle, R.: The modern-era retrospective analysis for research and
548 applications, version 2 (MERRA-2), J. Clim., 30, 5419-5454, 2017.
549 Ghahramani, Z.: Probabilistic machine learning and artificial intelligence, Nature, 521, 452-459,
550 2015.
551 Gneiting, T. and Raftery, A. E.: Weather forecasting with ensemble methods, Science, 310, 248-
552 249, 2005.



- 553 Goodfellow, I., Bengio, Y., Courville, A., and Bengio, Y.: Deep learning, 2, MIT press
554 Cambridge2016.
- 555 Gruber, A., Dorigo, W. A., Crow, W., and Wagner, W.: Triple collocation-based merging of satellite
556 soil moisture retrievals, *IEEE Transactions on Geoscience and Remote Sensing*, 55, 6780-6792,
557 2017.
- 558 Gruber, A., Su, C.-H., Zwieback, S., Crow, W., Dorigo, W., and Wagner, W.: Recent advances in (soil
559 moisture) triple collocation analysis, *International Journal of Applied Earth Observation and*
560 *Geoinformation*, 45, 200-211, 2016.
- 561 Ham, Y.-G., Kim, J.-H., and Luo, J.-J.: Deep learning for multi-year ENSO forecasts, *Nature*, 573,
562 568-572, 2019.
- 563 Hersbach, H., Bell, B., Berrisford, P., Hirahara, S., Horányi, A., Muñoz-Sabater, J., Nicolas, J., Peubey,
564 C., Radu, R., and Schepers, D.: The ERA5 global reanalysis, *Q. J. Roy. Meteor. Soc.*, 146, 1999-2049,
565 2020.
- 566 Hochreiter, S. and Schmidhuber, J.: Long short-term memory, *Neural Comput.*, 9, 1735-1780, 1997.
- 567 Hoffman, M. D., Blei, D. M., Wang, C., and Paisley, J.: Stochastic variational inference, *Journal of*
568 *Machine Learning Research*, 14, 2013.
- 569 Hossain, M., Rekabdar, B., Louis, S. J., and Dascalu, S.: Forecasting the weather of Nevada: A deep
570 learning approach, 2015 international joint conference on neural networks (IJCNN), 1-6,
- 571 Huang, Y., Xue, J., Wan, Q., Chen, Z., Ding, W., and Zhang, C.: Improvement of the surface pressure
572 operator in GRAPES and its application in precipitation forecasting in South China, *Advances in*
573 *Atmospheric Sciences*, 30, 354-366, 2013.
- 574 Hwang, J., Orenstein, P., Cohen, J., Pfeiffer, K., and Mackey, L.: Improving subseasonal forecasting
575 in the western US with machine learning, *Proceedings of the 25th ACM SIGKDD International*
576 *Conference on Knowledge Discovery & Data Mining*, 2325-2335,
- 577 Jacoboni, C. and Lugli, P.: The Monte Carlo method for semiconductor device simulation, Springer
578 Science & Business Media2012.
- 579 Kendall, A. and Gal, Y.: What uncertainties do we need in bayesian deep learning for computer
580 vision?, *arXiv preprint arXiv:1703.04977*, 2017.
- 581 Kingma, D. P. and Ba, J.: Adam: A method for stochastic optimization, *arXiv preprint*
582 *arXiv:1412.6980*, 2014.
- 583 Kirtman, B. P., Min, D., Infanti, J. M., Kinter, J. L., Paolino, D. A., Zhang, Q., Van Den Dool, H., Saha,
584 S., Mendez, M. P., and Becker, E.: The North American multimodel ensemble: phase-1 seasonal-
585 to-interannual prediction; phase-2 toward developing intraseasonal prediction, *B. Am. Meteorol.*
586 *Soc.*, 95, 585-601, 2014.
- 587 Kobold, M. and Sušelj, K.: Precipitation forecasts and their uncertainty as input into hydrological
588 models, *Hydrol. Earth. Syst. Sc.*, 9, 322-332, 2005.
- 589 Kullback, S. and Leibler, R. A.: On information and sufficiency, *The annals of mathematical statistics*,
590 22, 79-86, 1951.
- 591 Linde, N., Ginsbourger, D., Irving, J., Nobile, F., and Doucet, A.: On uncertainty quantification in
592 hydrogeology and hydrogeophysics, *Adv. Water Resour.*, 110, 166-181,
593 <https://doi.org/10.1016/j.advwatres.2017.10.014>, 2017.
- 594 Loquercio, A., Segu, M., and Scaramuzza, D.: A general framework for uncertainty estimation in
595 deep learning, *IEEE Robotics and Automation Letters*, 5, 3153-3160, 2020.
- 596 Luo, Y., Zhang, R., Wan, Q., Wang, B., Wong, W. K., Hu, Z., Jou, B. J.-D., Lin, Y., Johnson, R. H., and



- 597 Chang, C.-P.: The southern China monsoon rainfall experiment (SCMREX), *B. Am. Meteorol. Soc.*,
598 98, 999-1013, 2017.
- 599 McColl, K. A., Vogelzang, J., Konings, A. G., Entekhabi, D., Piles, M., and Stoffelen, A.: Extended
600 triple collocation: Estimating errors and correlation coefficients with respect to an unknown target,
601 *Geophys. Res. Lett.*, 41, 6229-6236, 2014.
- 602 Metropolis, N. and Ulam, S.: The monte carlo method, *J. Am. Stat. Assoc.*, 44, 335-341, 1949.
- 603 Molinari, J. and Dudek, M.: Parameterization of convective precipitation in mesoscale numerical
604 models: A critical review, *Mon. Weather. Rev.*, 120, 326-344, 1992.
- 605 Nitzler, J., Biehler, J., Fehn, N., Koutsourelakis, P.-S., and Wall, W. A.: A generalized probabilistic
606 learning approach for multi-fidelity uncertainty propagation in complex physical simulations, arXiv
607 preprint arXiv:2001.02892, 2020.
- 608 Papacharalampous, G., Tyralis, H., Koutsoyiannis, D., and Montanari, A.: Quantification of predictive
609 uncertainty in hydrological modelling by harnessing the wisdom of the crowd: A large-sample
610 experiment at monthly timescale, *Adv. Water Resour.*, 136, 103470,
611 <https://doi.org/10.1016/j.advwatres.2019.103470>, 2020.
- 612 Parrish, M. A., Moradkhani, H., and DeChant, C. M.: Toward reduction of model uncertainty:
613 Integration of Bayesian model averaging and data assimilation, *Water Resour. Res.*, 48, 2012.
- 614 Pozzi, W., Sheffield, J., Stefanski, R., Cripe, D., Pulwarty, R., Vogt, J. V., Heim, R. R., Brewer, M. J.,
615 Svoboda, M., and Westerhoff, R.: Toward global drought early warning capability: Expanding
616 international cooperation for the development of a framework for monitoring and forecasting, *B.*
617 *Am. Meteorol. Soc.*, 94, 776-785, 2013.
- 618 Premoli, A. and Tavella, P.: A revisited three-cornered hat method for estimating frequency
619 standard instability, *IEEE Transactions on instrumentation and measurement*, 42, 7-13, 1993.
- 620 Reeves, H. D., Elmore, K. L., Ryzhkov, A., Schuur, T., and Krause, J.: Sources of uncertainty in
621 precipitation-type forecasting, *Weather and forecasting*, 29, 936-953, 2014.
- 622 Reichstein, M., Camps-Valls, G., Stevens, B., Jung, M., Denzler, J., and Carvalhais, N.: Deep learning
623 and process understanding for data-driven Earth system science, *Nature*, 566, 195-204, 2019.
- 624 Rubinstein, R. Y. and Kroese, D. P.: *Simulation and the Monte Carlo method*, John Wiley &
625 Sons 2016.
- 626 Saha, S., Moorthi, S., Wu, X., Wang, J., Nadiga, S., Tripp, P., Behringer, D., Hou, Y.-T., Chuang, H.-
627 y., and Iredell, M.: The NCEP climate forecast system version 2, *J. Clim.*, 27, 2185-2208, 2014.
- 628 Sahoo, S., Russo, T., Elliott, J., and Foster, I.: Machine learning algorithms for modeling groundwater
629 level changes in agricultural regions of the US, *Water Resour. Res.*, 53, 3878-3895, 2017.
- 630 Schiavazzi, D. E., Doostan, A., Iaccarino, G., and Marsden, A. L.: A generalized multi-resolution
631 expansion for uncertainty propagation with application to cardiovascular modeling, *Computer*
632 *Methods in Applied Mechanics and Engineering*, 314, 196-221,
633 <https://doi.org/10.1016/j.cma.2016.09.024>, 2017.
- 634 Shi, X., Chen, Z., Wang, H., Yeung, D.-Y., Wong, W.-K., and Woo, W.-c.: Convolutional LSTM
635 network: A machine learning approach for precipitation nowcasting, arXiv preprint
636 arXiv:1506.04214, 2015.
- 637 Sikder, S. and Hossain, F.: Assessment of the weather research and forecasting model generalized
638 parameterization schemes for advancement of precipitation forecasting in monsoon-driven river
639 basins, *Journal of Advances in Modeling Earth Systems*, 8, 1210-1228, 2016.
- 640 Sønderby, C. K., Espeholt, L., Heek, J., Dehghani, M., Oliver, A., Salimans, T., Agrawal, S., Hickey, J.,



- 641 and Kalchbrenner, N.: Metnet: A neural weather model for precipitation forecasting, arXiv preprint
642 arXiv:2003.12140, 2020.
- 643 Srivastava, N., Hinton, G., Krizhevsky, A., Sutskever, I., and Salakhutdinov, R.: Dropout: a simple way
644 to prevent neural networks from overfitting, *The journal of machine learning research*, 15, 1929–
645 1958, 2014.
- 646 Stoffelen, A.: Toward the true near-surface wind speed: Error modeling and calibration using triple
647 collocation, *Journal of geophysical research: oceans*, 103, 7755–7766, 1998.
- 648 Sudret, B., Marelli, S., and Wiart, J.: Surrogate models for uncertainty quantification: An overview,
649 2017 11th European Conference on Antennas and Propagation (EUCAP), 19–24 March 2017, 793–
650 797, [10.23919/EuCAP.2017.7928679](https://doi.org/10.23919/EuCAP.2017.7928679),
- 651 Sun, Q., Miao, C., Duan, Q., Ashouri, H., Sorooshian, S., and Hsu, K. L.: A review of global
652 precipitation data sets: Data sources, estimation, and intercomparisons, *Rev. Geophys.*, 56, 79–107,
653 2018.
- 654 Taylor, K. E., Stouffer, R. J., and Meehl, G. A.: An overview of CMIP5 and the experiment design, *B.*
655 *Am. Meteorol. Soc.*, 93, 485–498, 2012.
- 656 Trebing, K., Stańczyk, T., and Mehrkanoon, S.: Smaat-unet: Precipitation nowcasting using a small
657 attention-unet architecture, *Pattern Recog. Lett.*, 145, 178–186, 2021.
- 658 van den Hurk, B., Doblas-Reyes, F., Balsamo, G., Koster, R. D., Seneviratne, S. I., and Camargo, H.:
659 Soil moisture effects on seasonal temperature and precipitation forecast scores in Europe, *Clim.*
660 *Dynam.*, 38, 349–362, 2012.
- 661 Vitart, F., Ardilouze, C., Bonet, A., Brookshaw, A., Chen, M., Codorean, C., Déqué, M., Ferranti, L.,
662 Fucile, E., and Fuentes, M.: The subseasonal to seasonal (S2S) prediction project database, *B. Am.*
663 *Meteorol. Soc.*, 98, 163–173, 2017.
- 664 Von Neumann, J. and Ulam, S.: Monte carlo method, *National Bureau of Standards Applied*
665 *Mathematics Series*, 12, 36, 1951.
- 666 Wei, K., Ouyang, C., Duan, H., Li, Y., Chen, M., Ma, J., An, H., and Zhou, S.: Reflections on the
667 catastrophic 2020 Yangtze River Basin flooding in southern China, *The Innovation*, 1, 100038, 2020.
- 668 Xu, L., Chen, N., and Zhang, X.: Global drought trends under 1.5 and 2 C warming, *Int. J. Climatol.*,
669 39, 2375–2385, 2019.
- 670 Xu, L., Abbaszadeh, P., Moradkhani, H., Chen, N., and Zhang, X.: Continental drought monitoring
671 using satellite soil moisture, data assimilation and an integrated drought index, *Remote Sens.*
672 *Environ.*, 250, 112028, 2020a.
- 673 Xu, L., Chen, N., Moradkhani, H., Zhang, X., and Hu, C.: Improving Global Monthly and Daily
674 Precipitation Estimation by Fusing Gauge Observations, Remote Sensing, and Reanalysis Data Sets,
675 *Water Resour. Res.*, 56, e2019WR026444, 2020b.
- 676 Xu, L., Chen, N., Zhang, X., Moradkhani, H., Zhang, C., and Hu, C.: In-situ and triple-collocation
677 based evaluations of eight global root zone soil moisture products, *Remote Sens. Environ.*, 254,
678 112248, 2021.
- 679 Yuan, X., Liang, X.-Z., and Wood, E. F.: WRF ensemble downscaling seasonal forecasts of China
680 winter precipitation during 1982–2008, *Clim. Dynam.*, 39, 2041–2058, 2012.
- 681 Zheng, G., Li, X., Zhang, R.-H., and Liu, B.: Purely satellite data-driven deep learning forecast of
682 complicated tropical instability waves, *Science advances*, 6, eaba1482, 2020.
- 683 Zhu, Y. and Zabaras, N.: Bayesian deep convolutional encoder–decoder networks for surrogate
684 modeling and uncertainty quantification, *Journal of Computational Physics*, 366, 415–447,

<https://doi.org/10.5194/hess-2021-432>
Preprint. Discussion started: 25 August 2021
© Author(s) 2021. CC BY 4.0 License.



685 <https://doi.org/10.1016/j.jcp.2018.04.018>, 2018.